HHS Public Access

Author manuscript

Clin Cancer Res. Author manuscript; available in PMC 2021 March 20.

Published in final edited form as:

Clin Cancer Res. 2021 January 15; 27(2): 608–621. doi:10.1158/1078-0432.CCR-20-1610.

Blocking IL1 Beta Promotes Tumor Regression and Remodeling of the Myeloid Compartment in a Renal Cell Carcinoma Model: Multidimensional Analyses

David H. Aggen[1,2,6,*], **Casey R. Ager**[1], **Aleksandar Obradovic**[1], **Nivedita Chowdhury**[1], **Ali Ghasemzadeh**[1], **Wendy Mao**[1,3], **Matthew Chaimowitz**[1], **Zoila A. Lopez-Bujanda**[1,4], **Catherine S. Spina**[1,5], **Jessica E. Hawley**[6], **Matthew C. Dallos**[6], **Cheng Zhang**[7], **Vinson Wang**[1,8], **Hu Li**[5], **Xinzheng Guo**[1], **Charles G. Drake**[1,6,8,*]

[1.]Columbia Center for Translational Immunology, Columbia University Irving Medical Center, New York, NY USA 10032.

[2.]Current Address: Memorial Sloan Kettering Cancer Center, 1275 York Ave, New York, NY USA 10065

[3.]Current Address: Kite Pharma, 930 Clopper Rd Suite 200, Gaithersburg, MD USA 20878

[4.]Department of Pathology, Johns Hopkins University School of Medicine, Baltimore, MD, USA 21205

[5.]Department of Radiation Oncology, Columbia University Irving Medical Center, New York, NY USA 10032

[6.]Department of Hematology Oncology, Columbia University Irving Medical Center, New York, NY USA 10032

[7.]Department of Molecular Pharmacology and Experimental Therapeutics, Mayo Clinic, Rochester, MN USA 55905

[8.]Department of Urology, Columbia University Irving Medical Center, New York, NY USA 10032

Abstract

Purpose: Intratumoral immunosuppression mediated by myeloid-derived suppressor cells (MDSC) and tumor-associated macrophages (TAM) represents a potential mechanism of immune checkpoint inhibitor (ICI) resistance in solid tumors. By promoting TAM and MDSC infiltration, Interleukin-1 beta (IL-1β) may drive adaptive and innate immune resistance in renal cell carcinoma (RCC) and in other tumor types.

Experimental Design: Using the RENCA model of RCC, we evaluated clinically relevant combinations of anti-IL-1β plus either anti-PD-1 or the multi-targeted tyrosine kinase inhibitor

[*]**Corresponding Author:** Charles G. Drake, MD, PhD, cgd2139@cumc.columbia.edu, Herbert Irving Cancer Center, New York-Presbyterian/Columbia University Medical Center, 177 Fort Washington Avenue, 6GN-435, New York, NY 10032.

Conflict of Interest Disclosure Statement: DHA has served as a paid consultant to Boehringer Ingelheim. CGD is a co-inventor on patents licensed from Johns Hopkins University to Bristol Myers Squibb, and has served as a paid consultant to Agenus, AZ Medimmune, BMS, Compugen, Kleo, Pfizer, Roche, Sanofi Aventis, Genentech, Merck, and Janssen, and has received sponsored research funding to his institution from the Bristol-Myers Squibb International Immuno-Oncology Network.

(TKI) cabozantinib. We performed comprehensive immune profiling of established RENCA tumors by via multiparameter flow cytometry, tumor cytokine profiling, and single-cell RNA sequencing. Similar analyses were extended to the MC38 tumor model.

Results: Analyses via multiparameter flow cytometry, tumor cytokine profiling, and single-cell RNA sequencing showed that anti-IL-1β reduces infiltration of polymorphonuclear myeloid-derived suppressor cells (PMN-MDSCs) and tumor-associated macrophages (TAMs). Combination treatment with anti-IL-1β plus anti-PD-1 or cabozantinib showed increased anti-tumor activity that was associated with decreases in immunosuppressive MDSC and increases in M1-like TAM.

Conclusion/Discussion: Single-cell RNA sequencing analyses show that IL-1β blockade and ICI or TKI remodel the myeloid compartment through non-redundant, relatively T cell independent mechanisms. IL-1β is an upstream mediator of adaptive myeloid resistance and represents a potential target for kidney cancer immunotherapy.

Keywords

Interleukin-1 beta; Kidney Cancer; Myeloid-Derived Suppressor Cells; Single-Cell RNA sequencing; cabozantinib; tyrosine kinase inhibitor; TKI; immunotherapy

Introduction:

Renal cell carcinoma is the 8th most common cancer in the United States, with an estimated 68,000 deaths attributable to this disease in 2020.(1) Numerous studies showed that renal cell carcinoma is unresponsive to chemotherapy, yet relatively responsive to immunotherapies including high-dose interleukin-2.(2) Based on these clinical data, metastatic RCC represents a fertile ground to translate combinatorial approaches involving immune checkpoint inhibition (ICI). To that end, there are now 3 FDA approved regimens combining PD-1 or PD-L1 targeted therapeutics with additional agents for first-line treatment of patients with metastatic kidney cancer.(3)

The current standard-of-care treatment for first-line metastatic renal cell carcinoma involves either combination PD-1/CTLA-4 blockade(4) or combining an anti-PD-1/PD-L1 therapy with a vascular-endothelial growth factor (VEGF) targeted tyrosine kinase inhibitor (TKI) such as axitinib(5,6). While these combinatorial approaches show improved response rates and overall survival relative to treating with a single-agent TKI (sunitinib), approximately 40–60% of patients do not respond to first-line combination therapy. Even more striking, close to 50% of patients with metastatic RCC progress to the extent that they are unable to move on to a 2nd line treatment, highlighting the notion that maximizing efficacy in the front-line setting may improve overall survival.(7)

One potential reason for the failure of current combination approaches is the presence of immunosuppressive cell populations within the tumor microenvironment (TME) including myeloid-derived suppressor cells (MDSCs), M2-like tumor associated macrophages (TAM) and regulatory T cells (Treg) that prevent effective immune-mediated tumor rejection.(8) In human renal cell carcinoma, increased MDSC infiltration within the TME is associated with increased expression of a number of cytokines including interleukin-1β (IL-1β),

Interleukin-8 (IL-8), and CXCL5 and overall poor prognosis. Hence, targeting myeloid cells may represent a potential strategy to overcome tumor tolerance.(9)

One potential target to manipulate innate immune cells in RCC is IL-1β. (10,11) Intratumoral macrophages, monocytes, tumor cells, and tumor vasculature are all proposed sources of IL-1β, which has numerous pro-tumorigenic properties including inflammasome activation, promotion of tumor angiogenesis and recruitment of immunosuppressive cells like PMN-MDSCs.(12,13) Early studies with IL-1 knockout mice showed that tumor growth was nearly completed abrogated in mice lacking IL-1β, suggesting that at early stages of tumor growth IL-1β-mediates sterile inflammation to promote tumor invasiveness.(14) In preclinical models of breast cancer, IL-1β blockade decreased macrophage-mediated tumor immunosuppression, and combining anti-IL-1β with anti-PD-1 resulted in near complete tumor eradication. (15) In humanized breast cancer models, IL-1 was implicated in driving tumor-promoting inflammatory changes that were reversed with TGF-β or IL-1 blockade. (16) Similarly, transfection of CT26 tumors with IL-1β led to a 50-fold increase in polymorphonuclear MDSCs (PMN-MDSCs), suggesting that IL-1 promotes immunosuppressive cell infiltration.(17) In human xenograft models of kidney cancer, blocking the IL-1 receptor axis resulted in reduced pro-tumorigenic TAM and decreased *in vivo* tumor growth.(18) In the same study, gene expression analyses showed that IL-1β expression correlated with myelomonocytic markers and advanced tumor stage, suggesting that IL-1β may promote RCC tumor progression. Of note, the most common treatment for RCC, VEGF tyrosine kinase inhibition, has not been extensively modeled in combination with IL-1β blockade.

Recent clinical data from a large, double-blinded placebo-controlled trial evaluating the efficacy of IL-1β blockade in secondary cardiac prevention provide further support for testing IL-1β blockade in cancer. (19) CANTOS (Canakinumab Anti-Inflammatory Thrombosis Outcomes Study) was a randomized trial testing the ability of the IL-1β blocking antibody canakinumab to prevent recurrent vascular events in patients following a myocardial infarction.(19) The study met its primary cardiac endpoint, and a pre-specified secondary endpoint of CANTOS quantified lung cancer incidence and mortality.(20) These analyses showed that the total cancer incidence was strikingly lower in patients receiving canakinumab, with an estimated incidence per 100 person-years of 0.64 in the placebo group in comparison to 0.55, 0.40, and 0.31 in the canakinumab treated groups at doses of 50 mg, 150 mg, and 300 mg respectively (p trend =0.0007 across all treated patients as compared to placebo). Lung cancer mortality was also decreased in patients treated with the 300 mg dose of canakinumab in comparison to patients treated with placebo (HR 0.49). These preclinical and emerging clinical data support targeting IL-1β in cancer, but a paucity of data exist regarding the immune changes mediated by IL-1β blockade in combination with other therapeutics; i.e. to date, a single study evaluated the additive effects of combination PD-1/IL-1β blockade(15) and no such data exist in an RCC model. We hypothesized that combining IL-1β blockade with agents active in human RCC, anti-PD-1 or the multi-targeted tyrosine kinase inhibitor cabozantinib) would lead to delayed tumor outgrowth and to changes in the myeloid compartment of the TME in a murine model of RCC.

Here we analyzed the immunological effects of anti-IL-1β on intratumoral immune cell subsets and show that while anti-PD-1, cabozantinib, or anti-IL-1β monotherapy exert anti-tumor effects in established tumors, combination therapy with anti-PD-1 or cabozantinib plus anti-IL-1β led to a more significant reduction in tumor growth. This enhancement in anti-tumor response was associated with decreased intratumoral PMN-MDSCs and skewing of tumor-associated macrophages towards an M1-like phenotype. Deep immune profiling of treated tumors using multiparameter flow cytometry showed that combination treatment with cabozantinib plus anti-IL-1β has pronounced effects on intratumoral myeloid populations, suggesting that this combination may act through a relatively T cell independent mechanism. Together these data support the hypothesis that IL-1β may function as an important mediator of intratumoral immunosuppression and suggest that anti-IL-1β based combination regimens may have activity in patients with RCC.

Materials and Methods:

Cell Lines

The murine renal cell carcinoma line (RENCA) was obtained from American Type Culture Collection (ATCC, Manassas, VA). Cells were maintained in RPMI medium supplemented with 10% fetal calf serum (FCS) and penicillin/streptomycin with non-essential amino acids and L-glutamine (RPMI Complete). Cells were mycoplasma tested prior to implantation using PCR by ATCC.

Mice

Female BALB/C mice (6–8 weeks old) were purchased from the Jackson Laboratory. All mice were housed in micro-isolator cages and treated in accordance with NIH and American Association of Laboratory Animal Care Regulations. All mouse procedures and experiments for this study were approved by the Columbia University Medical Center Institutional Animal Care and Use Committee (IACUC) Regulations. Ten to fifteen mice per treatment group were used in tumor outgrowth studies; prior data in this model suggest these numbers provide a 90% power and a 5% significance level in terms of detecting differences in tumor volume.

Tumor challenge and treatment experiments.

On day 0, mice were injected subcutaneously (s.q.) in the right flank with 5×10^5 RENCA cells. On day +12, animals with well-established tumors measuring 25 – 50 mm^2 were treated with antibody therapeutics every 3 days x 2 doses as indicated. Treatments were given as single-agents or in combination, with the following regimens for each drug: anti-PD-1 (BioXCell, Cat #BE0146, Clone RMP1–14) 200 μg every 72 hours by i.p. injection, Anti-IL-1β (BioXCell, Cat #BE0246, Clone B122) 200 μg every 72 hours by i.p. injection, Cabozantinib (Selleck Chem, CAT #S1119, XL184, dissolved in 2% DMSO+ 30%PEG+ 5%Tween80+ddH20) at 3 mg/kg/mouse every 24 hours by oral gavage. Control antibodies included polyclonal Armenian hamster IgG (BioXCell, Cat # BE0091) at 200 μg every 72 hours by i.p. injection or rat IgG2a isotype control at 200 μg every 72 hours by i.p. injection. Vehicle treated mice in the cabozantinib group received 20 microliters of dilution buffer without cabozantinib. To minimize the number of mice utilized the anti-IL-1β and vehicle

treated mice were used as controls for experiments with both anti-PD-1 (Figure 1 and 2) and cabozantinib (figure 3 and 4). On Day +18 mice were sacrificed and spleen, tumor draining lymph node, and tumor were isolated as previously described.(21,22) Experiments in figures 1 and 3 were replicated at least 3 times. To minimize the number of mice used, vehicle and anti-IL-1b mice were used as controls performed simultaneously for the data in figures 1 and 3.

Flow Cytometry

Tumors were harvested and dissociated using the Miltenyi murine tumor dissociation kit (Cat #130-096-730) per the manufacturers protocol with a Gentlemacs dissociator (Miltenyi Inc Gaithersburg, MD). Single-cell suspensions were washed with PBS and incubated with ACK lysis buffer (3 cc for 3 min) and quenched with 45 cc PBS. To limit instrument and reagent use, 25% of each tumor lysate was used for subsequent flow cytometry experiments. Cells were incubated with Fc-block BD Biosciences, Woburn, MA, Cat #553141) and then stained with Near-IR Live dead and T cell or myeloid makers. For a myeloid cell panel, cells were stained with anti-Ly6G (BV421 anti-Ly6G, Clone 1A8, BD Biosciences, Cat #562737), anti-CD3 (BV786 anti-CD3, Clone 17A2, BD Biosciences, Cat #564010), anti-CD45 (BV510 anti-CD45, Clone 30-F11, BD Biosciences, Cat #563891), anti-MHC II (PE anti-MHC II, Clone M5/114.15.2, eBioscience, Cat #12-5321-82), anti-F4/80 (PE/Cy7, Clone BM8, BioLegend, Dedham, MA, Cat #123114), anti-Ly6C (APC anti-Ly6C, Clone HK1.4, BioLegend, Cat #128016), and anti-CD11b (AF700 anti-CD11b, Clone M1/70, BioLegend, Cat #101222). For a T cell panel, cells were stained with anti-CD45 (BV510 anti-CD45, Clone 30-F11, BD Biosciences, Cat #563891), anti-CD4 (BV650 anti-CD4, Clone RM4–5, BioLegend, Cat #00555), anti-CD8 (BV711 anti-CD8, BioLegend, Clone 53–6.7, Cat #100759), anti-LAG-3 (PE eBioscience, Clone C9B7W, Cat #12-2231-83), anti-PD-1 (PE/Cy7 anti-CD279 (anti-PD-1), Biolegend, Clone 29F.1A12, Cat #135216), anti-TIM-3 (APC anti-CD366 (TIM-3), Biolegend, Clone RMT3–23, Cat #119706), and anti-CD11b (AF700 anti-CD11b, Clone M1/70, BioLegend, Cat #101222). For intracellular staining, cells were fixed and permeabilized using the Invitrogen eBioscience Foxp3/ Transcription Factor Staining buffer set (ThermoFisher Scientific Cat. #00-5523-00, Waltham, MA) per the manufacturer's protocol. For a T cell panel, single cell suspensions were stained with PE anti-FOXP3 (Clone FJK-16s, eBioscience/Thermofisher) and AlexaFluor647 anti-CTLA-4 (Clone L3D10, BioLegend, Dedham, MA) per the manufacturer's protocol.

RNA sequencing

Tumors were harvested, dissociated and washed as for flow cytometry experiments. Cells were stained with Near-IR live/dead (Thermo/Fisher Cat #L10119) and BV650 anti-CD45 (BioLegend, CAT #103151, Clone 30-F11) and CD45+ cells isolated by FACS using a BD Influx Instrument (BD Biosciences, Woburn, MA). RNA was isolated using Qiagen RNAeasy Mini Kit (Cat #74134, Qiagen, Frederick, MD). RNA sequencing was performed in the Genome Analysis core at Mayo Clinic. Sequence reads were aligned to the mouse reference genome.(23)

Cytokine Analyses:

Tumors were excised, snap-frozen in liquid nitrogen, resuspended in 500 μL MSD TRIS Lysis Buffer (Mesoscale Discover, Cat #R60TX-3, Rockville, MD) and pulverized using stainless steel beads (Qiagen, Cat #69989) in a Tissue-Lyser II (Qiagen) set at 2 × 30 seconds at 20 Hz. Samples were centrifuged at 14000 rpm for 10 min at 4 degrees C. Supernatant was transferred and stored at −80 in aliquots. Protein was quantified using the Bradford Assay, and 250 μg of total protein was used in triplicate for quantification of cytokines using the mesoscale MESO QuickPlex SQ 120 instrument, (Mesoscale, Rockville, MD). For these experiments, the U-Plex 10-Plex Kit, was used; this includes the Cytokines: IFNγ, IL-1β, IL-2, IL-4, IL-5, IL-6, IL-10, IL-12p70, KC/GRO, and TNFα). To conserve animals, the vehicle and anti-IL-1β treated sorted immune cells were from the same animals in the experiments detailed in figures 2 and 4.

Single Cell Gene Expression Analysis:

Single-cell suspensions were generated as for flow cytometry using the Miltenyi Gentlemacs per the manufacturer's instructions from tumors treated with vehicle, cabozantinib, or cabozantinib + anti-IL-1β (n=3/treatment group). As described above, CD45+ cells were isolated by fluorescence-activated cell sorting and loaded as a gel emulsion into the Chromium 10x platform per manufacturer's instructions (10x Genomics, Pleasanton, CA). Unique Molecular Identifier (UMI) counts per gene for each cell were obtained on a sample-by-sample basis using the 10X cellranger pipeline, and then merged for downstream analysis using Seurat v3. Cells were quality-control filtered to exclude those with coverage of less than 500 genes and those where mitochondrial genes representing more than 5% of total UMI count. UMI counts for high-quality cells were then log-normalized and scaled. Clustering was performed using the Louvain algorithm, with top genes per cluster identified by combined likelihood ratio test for single-cell gene expression.(24) For ease of cluster phenotyping, the top gene sets were separately filtered to include only statistically significant cluster-specific immune-relevant genes enumerated by the I/O 360 Nanostring platform (Nanostring Technologies, Seattle, WA).(25)

Spectral Cytometry:

Single-cell suspensions were stained with extracellular antibodies as shown in supplemental table 2. Cells were then washed, fixed, and permeabilized using the Invitrogen eBioscience Foxp3/Transcription Factor Staining buffer set (ThermoFisher Scientific Cat. #00-5523-00) per the manufacturer's protocol. Cells were next stained with antibodies to intracellular markers. Single stain controls were performed using UltraComp eBeads (ThermoFisher Scientific Cat #01-2222-41) and samples were unmixed using CyTEK Aurora software (Cytek corporation, Fremont, CA). Sample files were cleaned, downsampled (5×10^4 live CD45+ cells per sample), and concatenated using FlowJo (v10, Becton Dickinson, East Rutherford, NJ). Nonlinear dimensionality reduction was performed on concatenated samples using either the t-distributed Stochastic Neighbor Embedding (tSNE) implementation within FlowJo v10 or visual interactive Stochastic Neighbor Embedding (viSNE) within Cytobank (relevant parameters: 5000 iterations, k=50). Unbiased clustering was performed using the Phenograph and FlowSOM Plug-ins in FlowJo, and further

downstream data processing, heatmap generation and statistical analyses were performed in FlowJo, Excel 2016, and GraphPad Prism 8.

Results:

Combination Treatment With αIL-1β Plus αPD-1 Delays Tumor Growth

To evaluate the anti-tumor activity of anti-IL-1β, we used late, well-established subcutaneous RENCA tumors, as RENCA represents one of the few syngeneic RCC models available. On day +12 post implantation, when tumors were palpable at approximately 25–50 mm^3, animals were treated with anti-IL-1β alone or in combination with anti-PD-1 (Figure 1A). Of note, the RENCA tumor model is generally moderately resistant to anti-PD-1 monotherapy. (26) We found that anti-IL-1β monotherapy significantly delayed tumor growth, and that combining anti-IL-1β with anti-PD-1 further delayed tumor progression (Figures 1B–C),

Anti-IL-1β Alters the Myeloid Cell Compartment of the Tumor Microenvironment (TME)

To understand the immunological effects on both lymphocytes and myeloid cells in anti-IL-1β treated tumors, we quantified immune cell subsets by flow cytometry. Immunophenotyping showed that blocking IL-1β did not significantly alter the percentages of CD8, CD4, or regulatory T cell infiltrates in the TME (Figure 1D). To analyze the phenotype of these T cell populations, we used high-dimensional spectral cytometry; those data are shown in Figure 6 and Supplemental Figure 3 and are discussed below.

Myeloid derived suppressor cells (MDSCs) constitute a major component of the immunosuppressive TME and are increased in number in established RENCA tumors.(27). In contrast to its effects on T cells, anti-IL-1β significantly decreased infiltration of granulocytic cells as defined by expression of CD11b, $Ly6G^{hi}$ and $Ly6C^{int}$; this was also noted in the context of anti-IL-1β plus anti-PD-1 combination treatment (Figure 1E). These data suggest that IL-1β blockade may block the expansion or recruitment of immunosuppressive PMN-MDSC to the TME. However, it should be noted these markers cannot definitively differentiate between neutrophils and PMN-MDSCs.(28,29). By contrast, monocytic-MDSCs within the TME, as defined as $CD11b^{+}$ $Ly6C^{hi}$ $Ly6G^{-}$ and $MHC\text{-}II^{+}$, were relatively unchanged by monotherapy or combination anti-IL-1β plus anti-PD-1 treatment. Quantification of tumor-associated macrophages (TAMs) showed that IL-1β blockade skewed polarization towards an M1-like phenotype as broadly defined by class II MHC expression. Further, anti-IL-1β plus anti-PD-1 combination therapy increased M1-like TAM infiltration relative to either monotherapy. To more deeply analyze the phenotype of these myeloid populations, we used high-dimensional spectral cytometry; those data are shown and discussed in Figure 6 below. Taken together, these data suggest that IL-1β blockade modulates PMN-MDSCs and promotes M1 TAM prevalence in the TME, and that these effects are potentiated in the presence of anti-PD-1.

Interleukin-1β Blockade Modulates Gene and Protein-Level Expression of Multiple Cytokines and Chemokines

Based on the results above, we hypothesized that IL-1β blockade might drive distinct gene expression profiles within myeloid and lymphoid cell populations. To test that hypothesis, we isolated CD45+ tumor infiltrating cells using FACS, and performed gene expression profiling by RNAseq on those sorted populations. We found that anti-IL-1β monotherapy led to decreased expression of several cytokine genes, including IL-1β and IL-6 (Figure 2A). Although there is no direct murine homolog to human IL-8, *Cxcl1*, *Cxcl2*, *Cxcl12*, *MIP-1alpha* and *KC/GRO* are murine surrogates with homology to human IL-8 and have been proposed as potential surrogates of murine IL-8. (30–33) Treatment with anti-IL-1β led to decreased gene expression of *Cxcl2*, *Cxcl12*, and *KC/GRO* (Figure 2A) suggesting that IL-1β may lay upstream of these surrogates of IL-8; i.e. that IL-1β expression may drive IL-8 expression, ultimately resulting in PMN-MDSC recruitment to the TME.(34) Conversely, treatment with anti-PD-1 monotherapy was associated with relative up-regulation of *Cxcl2*, *Cxcl12*, and *IL-6*. To evaluate potential changes in genes involved in angiogenesis, we performed GSEA analysis using a well-described angiogenesis gene signature from the gene ontology database (Supplemental Figure 1).(35,36) These analyses showed that anti-IL-1β blockade, alone or in combination with anti-PD-1, demonstrated statistically significant decreases angiogenesis pathway transcripts.

To validate treatment-associated changes in cytokine levels at the protein level we used the Meso Scale Discovery (MSD) multiplex cytokine detection platform on tumor lysates from mice treated as in Figure 2A, and found that combination treatment with anti-IL-1β plus anti-PD-1 decreased intratumoral IL-1β protein expression (Figure 2B), consistent with the message level data. In addition, anti-IL-1β plus anti-PD-1 combination treatment decreased intratumoral levels of KC/GRO, a potential homolog of human IL-8, and was associated with decreased IL-10 levels. There was a trend towards increased intratumoral IFNγ and TNFα with anti-IL-1β plus anti-PD-1 combination therapy, but these changes did not reach statistical significance. Taken together, these data also suggest that IL-1β may be an upstream driver of multiple suppressive cytokines in RCC.

Combination Treatment with αIL-1β Plus Cabozantinib Delays Tumor Growth

Given the well-established efficacy of VEGF-TKI treatment in RCC (37), we tested whether combining anti-IL-1β with a VEGF-TKI would have additive or potentially synergistic anti-tumor effects, and whether these effects were analogous to those observed in immunotherapy combination studies above. For these studies we chose cabozantinib, which is commonly used in second-line treatment of RCC. Our choice of cabozantinib was further driven by its activity as a relatively broad-spectrum TKI, with activity against c-MET, RET, KIT, AXL, and FLT3 in addition to VEGFR2. (38) The treatment scheme is for these studies is shown in Figure 3A. We found that both anti-IL-1β and cabozantinib delayed tumor outgrowth, with further inhibition noted in animals treated with anti-IL-1β plus cabozantinib combination therapy (Figures 3A,B). We also tested cabozantinib, anti-IL-1β, and combination cabozantinib/anti-IL-1β treatment in the MC38 colorectal cancer model, and did not observe statistically significant changes in tumor outgrowth in this model, likely

reflecting differences in the baseline myeloid infiltrate in this murine model relative to RENCA (Supplemental Figure 9A and 9B).

Anti-IL-1β Plus Cabozantinib Combination Treatment Decreases PMN-MDSCs and Promotes M1 TAM

We next quantified key immune cell populations in the TME using flow cytometry. While no statistically significant changes were noted in CD8, CD4, or Treg infiltration across treatment groups, a non-significant trend towards decreased intratumoral regulatory T cells was observed with either cabozantinib or anti-IL-1β plus cabozantinib combination treatment (Figure 3D). Unlike anti-IL-1β, treatment with cabozantinib did not alter intratumoral PMN-MDSC infiltration. (Figure 3E), however the reduction in PMN-MDSC mediated by anti-IL-1β monotherapy was maintained in the presence of cabozantinib, and was similar to that noted with combination anti-IL-1β plus anti-PD-1 combination therapy (Supplemental Figure 2C). Quantification of monocytic-MDSCs showed no differences in intratumoral predominance across treatment groups. Combining cabozantinib with anti-IL-1β increased M1-like TAM within the TME; importantly this effect was more pronounced than observed with anti-IL-1β plus anti-PD-1 (Supplemental Figure 2D). Deep immune profiling was also performed in the MC38 treatment model, there we found less profound changes in the myeloid and lymphoid compartment of the TME with cabozantinib and anti-IL-1β therapy (Supplemental Figure 9C – 9G). Taken together, these data support the notion that in addition to anti-PD-1, anti-IL-1β also has anti-tumor activity in combination with cabozantinib in the RENCA model, and that the anti-IL-1β plus cabozantinib combination may preferentially modulate TAM in tumor models with a higher degree of myeloid infiltration.

Anti-Interleukin-1β +/− Cabozantinib Modulates Gene and Protein-Level Expression of Multiple Cytokines and Chemokines

Using the methods outlined in Figure 2, we performed RNA sequencing of sorted CD45+ cells to more broadly understand the immune effects of anti-IL-1β plus cabozantinib combination treatment. The effects of anti-ILβ therapy were similar to those observed previously (Figure 2A); whilst cabozantinib monotherapy appeared to increase message-level expression of numerous cytokines including IL-1β, an opposite effect to that seen with anti-PD-1. Expression of several other cytokines appeared to be increased at the message level by cabozantinib; these include *IL-6*, *IL-10*, *CXCL1*, *CXCL2* (a potential murine IL-8 homolog), and *Cxcr2*, a receptor for IL-8 in humans (Figure 4A). Conversely, cabozantinib monotherapy decreased message-level expression level of Ly6C, which is associated with PMN-MDSC. Interestingly, the pro-immunogenic effects of anti-IL-1B dominated in the combination group of anti-IL-1β plus cabozantinib combination treatment where we observed decreased expression of *IL-1β*, *IL-6*, *Cxcl1*, and *CXCL2*. Gene set enrichment analysis to assess the relative angiogeneic effects of cabozantinib and anti-IL-1β did not show statistically significant differences in key angiogenesis genes (Supplemental Figure 1E).

We further interrogated these effects at the protein level, using the MSD discovery platform as in Figure 2B. At the protein level, cabozantinib treatment did not significantly increase

IL-1β intratumoral protein expression (Figure 4B), suggesting a possible disconnect between message and protein levels. However, anti-IL-1β plus cabozantinib significantly decreased IL-1β levels, as well as levels of the IL-8 homologue KC/GRO. Consistent with the data in Figure 2B, IFNγ levels were not significantly increased by IL-1β monotherapy; and the increased IFNγ noted with anti-IL-1β plus anti-PD-1 was not observed with anti-IL-1β plus cabozantinib. Taken together these data suggest that anti-IL-1β has significant anti-tumor effects in several combination regimens, and that those effects may be driven by disparate mechanisms.

Single-Cell Analyses of anti-IL-1β +/− Cabozantinib

To develop a more comprehensive understanding of the broader effects of these agents on the TME, we performed single-cell RNA sequencing on CD45+ cells sorted from RENCA tumors treated with vehicle, cabozantinib, and cabozantinib plus anti-IL-1β. Sorted cells were sequenced to an average read depth of > 1200 transcripts per cell with the aim of defining cellular phenotypes. Clustering using Seurat V3.0 identified 13 distinct clusters (Figure 5A, Supplemental Figures 4–6), of these clusters 1, 4, 8 and 12 demonstrated significant changes in prevalence between cabozantinib versus the anti-IL-1β plus cabozantinib groups (Figure 5B). Evaluation of the most highly upregulated genes in clusters 1–13 identified 2 clusters corresponding to T cells (cluster 6 and 8) and 11 clusters corresponding to cells of the myeloid lineage (Figure 5C). Clusters 0–5 had relatively high expression of ADGRE consistent with intratumoral TAM. Clusters 9–13 defined granulocytic, monocytic, NK cells, and B cell populations as indicated. Inspection of the most highly expressed genes within each cluster suggested that clusters 1, 4 and 12 correlate with intratumoral TAM, and cluster 8 with T cells (Supplemental Figure 6). To more deeply interrogate expression changes within each cluster, the top 15 genes from clusters 1, 4, 8, and 12 were determined (Figure 5C, Supplemental Figure 7). These data show that treatment with cabozantinib resulted in upregulation of complement genes including *C1qa* and *C1qb*, and the macrophage specific gene *TREM2* in clusters 1 and 4. Within cluster 12, the combination of cabozantinib and anti-IL-1β showed decreased expression of *Cxcl1, Cxcl2*, and *IL-1β* consistent with bulk RNA sequencing of sorted immune cells (Figure 4). Taken together these data show that the combination of cabozantinib and anti-IL-1β promotes myeloid remodeling across multiple intratumoral populations.

High-Dimensional Flow Cytometry Reveals Distinct Changes within CD4+ T Cells and Myeloid Cells with Combination Anti-IL-1β Therapy

To better understand which immune cell populations in the TME are modulated anti-IL-1β monotherapy and combination therapies (and how they correlate with treatment effects), we optimized a 24-parameter flow cytometry panel to facilitate simultaneous myeloid and T cell profiling (Supplemental Table 2). Using this panel, we analyzed treated tumors, and then performed unbiased dimensionality reduction using the tSNE algorithm (Figure 6A). These data broadly defined myeloid and lymphoid populations (Figure 6B and 6F). We next performed a second, dependent tSNE analysis of each compartment along with unbiased clustering using the Phenograph and FlowSOM algorithms. These data revealed 21 distinct myeloid cell clusters (Figure 6C) and 21 lymphoid clusters (Figure 6G) across treatment groups (Supplemental Table 1). The relative MFI for each protein marker for myeloid

(Figure 6C) and lymphoid markers (Figure 6G) defines each specific cluster. We next normalized the frequency of each cluster to its prevalence in vehicle-treated tumors, to determine which cell populations were affected by each treatment in both the myeloid (Figure 6D) and lymphoid compartment (Figure 6H). To identify statistically significant changes between cluster frequency and treatment group, 2-way ANOVA of selected treatment comparisons was performed (Figure 6E).

We first sought to identify anti-IL-1β driven effects on intratumoral myeloid cells (Figure 6D). Treatment with anti-IL-1β was associated with a decrease in Ly6G+, Ly6C−, CD11b dim cells (Cluster 1 and 3), consistent with a granulocytic or PMN-MDSC lineage. Anti-IL-1β therapy also increased M1 like TAM defined as MHC I high, iNOS high cells (Cluster 5 and 15). Similarly, treatment with anti-PD-1 resulted in a decrease in PMN-MDSCs (Clusters 1 and 3). Cabozantinib monotherapy decreased cluster 1 PMN-MDSCs and led to a >2-fold log increase in M1-like TAM in clusters 10, 17, and 20 (Figure 6D). These data support that anti-IL-1β, anti-PD-1, and cabozantinib exert significant changes within the myeloid compartment, and that cabozantinib monotherapy induced intratumoral M1-like TAM.

We next performed similar immunophenotyping for combination therapy with anti-IL-1β+ anti-PD-1 relative to vehicle alone (Figure 6E). With combination treatment, statistically significant decreases in PMN-MDSC clusters 1, 3, and 6 ($P < 0.05$ Figure 6E, 3rd row) and increases in the prevalence of M1 like TAM (clusters 10, 14, and 15) were noted by 2-way ANOVA ($P<0.05$, Figure 6E, 3rd row). The phenotypic changes within the macrophage and granulocytic compartment were more pronounced with combination therapy than with either anti- anti-IL-1β or anti-PD-1 monotherapy alone.

Perhaps most striking was the degree to which combination anti-IL-1β and cabozantinib increased M1-like TAM predominance within the TME, i.e. combination anti-IL-1β plus cabozantinib significantly increased M1-like TAM (clusters 10 and 14, $P<0.001$ and $P<0.01$ respectively) and decreased M2-like TAM (MHC II low, F4/80 DIM, Cluster 18, $P < 0.01$) relative to cabozantinib therapy alone (Figure 6E). Statistical analysis of each cluster frequency between all treatment groups using two-way ANOVA with Tukey's correction for multiple comparisons confirmed that observed changes in PMN-MDSC (cluster 1) and M1-like TAM (cluster 10) in the combination cabozantinib and anti-IL-1β group were significantly different as relative to vehicle-treated tumors and monotherapy treated controls (Figure 6E).

Based on the observed phenotypic changes in the myeloid compartment, we also performed phenotyping of T lymphocytes from tumors treated with anti-IL-1β, anti-PD-1, or cabozantinib monotherapy (Figures 6G, 6H, and 6E at right). Deeper immune profiling of the lymphocyte compartment identified less pronounced phenotypic changes within CD4 and CD8 immune cell subsets as relative to the myeloid compartment but identified additional differences that were not apparent in prior flow analysis using more basic panels (Figure 1, 3). We observed increases in CD8+, CCR7+, CD62L low cells (cluster 20) and CD4+, CCR7+, CD62L low T cells (cluster 21) with anti-IL-1β, anti-PD-1, and cabozantinib monotherapy relative to vehicle, respectively.

We then performed similar phenotypic analyses with combination anti-PD-1 and anti-IL-1β treated tumors. Similar to observations with anti-PD-1 monotherapy and anti-IL-1β monotherapy, increases in the frequency of cluster 20 and 21 T cells were noted. Analysis of combination cabozantinib and anti-IL-1β therapy showed a statistically significant increase in cluster 21 CD4+, CCR7+, CD62L+ T cells, suggesting that combination cabozantinib and anti-IL-1β therapy promoted the most significant CD4+ effector T cell response in this model. Similar analyses from lymphocytes within the tumor draining lymph node showed an increase in naïve T cells within the tumor draining lymph node with combination cabozantinib and anti-IL-1β (CD62 L hi, CD44 lo, cluster 7 and 25, Supplemental Figure 3). Together these data support that anti-IL-1β monotherapy exerts relatively minor changes within the T cell compartment.

Taken together, these profiling data support the conclusion that anti-IL-1β promotes M1-like anti-tumor TAM (Clusters 10 and 18), and decreases PMN-MDSC within the TME (Cluster 1). While these effects are potentiated to some effect in combination with anti-PD-1, combination treatment with cabozantinib and anti-IL-1β therapy promotes more robust M1-like TAM within the TME. Overall, in the RENCA model, the anti-tumor effects of cabozantinib + anti-IL-1β correlate with effects on MDSC and TAM, along with an increase in CD4+ CCR7+ effector T cells.

Discussion:

Chronic inflammation is a recognized promoter of tumor invasiveness and progression, dating back to early observations from Virchow in the 1800s.(39) Dampening chronic inflammation while leaving T cell functionality intact is a formidable challenge in an era where immune checkpoint blockade is a pillar of cancer treatment for several tumor types.(40) We found that anti-IL-1β delayed tumor outgrowth in an established RCC model. The anti-tumor effects of IL-1β blockade appear to be additive with immune checkpoint blockade using anti-PD-1 in the RENCA model, which is relatively resistant to anti-PD-1 therapy. These data are broadly consistent with results in immune-responsive tumor models evaluating IL-1β blockade.(15) In combination with anti-PD-1, the immunogenic effects of interleukin-1β blockade appear to primarily affect the myeloid compartment, suggesting that interleukin-1β and anti-PD-1 might have non-redundant and complementary mechanisms of action, and that targeting interleukin-1β might be a candidate approach to overcome adaptive immune resistance.

Clinically, a majority of patients with metastatic RCC receive anti-PD-1 or anti-PD-L1 immunotherapy in combination with either anti-CTLA-4 or the VEGF-TKI axitinib as front-line therapy. We showed that the myeloid effects of the VEGF-TKI cabozantinib are augmented by the addition of anti-IL-1β through targeting of both immunosuppressive MDSCs and reprogramming of TAMs. Combining cabozantinib with anti-IL-1β decreased tumor growth, with an associated decrease in PMN-MDSC infiltration. Immunophenotypic analysis by flow cytometry and by single-cell RNAseq showed that the immunogenic effects of combination cabozantinib and anti-IL-1β in this tumor model are also associated with significant changes in the myeloid compartment, manifest as a decrease in intratumoral PMN-MDSCs. Further, cabozantinib in combination with anti-IL-1β decreased tumor

outgrowth and led a significant increase in M1-like TAM within the TME. To our knowledge, this is the first study to illustrate potential synergy between anti-IL-1β blockade and a VEGF-targeted TKI.

We also found that the intratumoral cytokine profile within the TME is shifted with anti-IL-1β blockade. Systemic therapy with anti-IL-1β decreased transcript level expression of several cytokines including IL-6, CXCL2, CXCL12, KC/GRO. These transcriptional profiles have consequences for the intratumoral cytokine milieu, as anti-IL-1β alone decreased protein levels of IL-6 and homologs of IL-8 (KC/GRO). These data are consistent with work from several groups illustrating that interleukin-1β promotes increased IL-6 expression, but to our knowledge this is one of the first reports to suggest that IL-1 is an upstream mediator of homologues of IL-8.(41,42)

Furthermore, combination therapy with either anti-PD-1 or cabozantinib augmented the immunogenic effects of IL-1β blockade on intratumoral cytokines. The addition of anti-PD-1 to anti-IL1β further decreased transcript level expression of several downstream intratumoral cytokines that are upregulated with anti-PD-1 monotherapy including IL-10 and TNF-α, however, decreases of in IL-10 and TNF-α were not reflected at the protein level due to variation in protein quantification. Similar effects on intratumoral cytokine profiles were observed with combination cabozantinib and anti-IL-1β with statistically significant decreases in IL-6 and the IL-8 homolog KC/GRO. Gene expression analysis was also performed to assess the relative effects of IL-1β on angiogenesis based on the known contribution of IL-1β to the vascular endothelium (Supplemental Figure 1). Treatment with anti-IL-1β alone or in combination with anti-PD-1 led to statistically significant decreases in key angiogenesis genes within immune cells (Supplemental Figure 1A, 1C), consistent with observations from protein level cytokine quantification within the TME. In contrast, combination cabozantinib and anti-IL-1β did not significantly alter the angiogenesis gene signature relative to cabozantinib monotherapy (P=0.19). In terms of the leading edge genes (Figure 1B and 1D), comparison of anti-IL-1β relative to vehicle and anti-IL-1β /anti-PD1 vs. anti-PD1 showed downregulation of several angiogenic genes. These data suggest that IL-1β may also dampen angiogenic effects as monotherapy or when combined with immune checkpoint blockade. Overall, these data show that anti-IL-1β has differential effects on angiogenesis genes that depend on the context for rationale combination therapy, and support the hypothesis that IL-1β blockade has immunogenic effects in combination with cabozantinib. This observation suggests a potential mechanism for additive anti-tumor effects with either immune checkpoint blockade or a TKI.To this end, several downstream targets of IL-1β including IL-6 (43,44), IL-8 (45), and TNF-α (46) are being targeted in clinical trials with the goal of augmenting the anti-PD-1 immunotherapy response. Together, these findings support the notion that IL-1β may be an upstream regulator of adaptive myeloid resistance, and that IL-1β blockade may have the potential to reverse immunosuppressive cytokine programs that prevent successful anti-tumor immunity.

We also studied IL-1β mediated changes within the myeloid cell compartment in the RENCA model by performing deep immune profiling of sorted populations by both single-cell RNAseq and flow cytometry. Using single-cell RNA sequencing we delineated 13 unique clusters of immune cells. Treatment with cabozantinib or cabozantinib and anti-

IL-1β showed changes within the frequency of 3 distinct myeloid clusters (Clusters 1, 4, and 12) consistent with earlier flow cytometry data suggesting that both treatments remodel the myeloid compartment. Using spectral flow cytometry, we identified 21 distinct clusters of myeloid and lymphoid cells. These analyses also identified a potentially important population of CD4+, CCR7+, CD62 Low effector T cells which were most prevalent within the TME following cabozantinib plus anti-IL-1β combination therapy. The presence of CCR7+ T cells within the TME is consistent with skewing of the T cell compartment towards central memory phenotypes, which in some contexts are associated with anti-tumor response to immune checkpoint blockade.(47,48). Further, and consistent with recent data from a murine model of combined CTLA-4 / PD-1 blockade(49) as well as deep phenotyping of the human RCC TME(50), our immune cell clustering data show that the populations in the RENCA TME are more complex than those previously defined using markers of canonical immune subsets.

Overall, our results are consistent with prior observations that anti-IL-1β has anti-tumor properties, and that IL-1β blockade is potentially additive or synergistic with immune checkpoint blockade.(15) Consistent with observations from earlier studies in which overexpression of IL-1β increased MDSC infiltration within mammary carcinomas (51), we observed decreased intratumoral PMN-MDSCs following anti-IL-1β treatment. In other studies evaluating immune checkpoint blockade with anti-IL-1β, tumor eradication was in part dependent on CD8 cells, as CD8 T cell depletion rendered IL-1β knockout ineffective. (15) While we found less pronounced differences in CD8 T cells, this discrepancy is likely model dependent since other studies utilized the 4T1 tumor model, which is fairly responsive to anti-PD-1 therapy. Consistent with this, CD8 T cell depletion in the RENCA tumor model had little effect on the efficacy of combination cabozantinib and anti-IL-1β therapy (Supplemental Figure 8). Our data also support the hypothesis that targeting IL-1β in established tumors results in anti-tumor M1 like TAM infiltrates and a decrease in intratumoral PMN-MDSCs. It remains an open question whether anti-IL-1β decreases migration of PMN-MDSC to the TME, or whether the decreased prevalence noted by us and others reflects decreased local polarization.

Several studies have attempted to address the duality of interleukin-1β (52) in promoting tumor progression in certain models, whereas in other models interleukin-1β expression for cancer is required for tumor eradication.(52–54) When administered at supraphysiologic levels, IL-1β has the potential to induce both T_H1 and T_H17 responses with anti-tumor properties. (52) Indeed, tumor regression is observed with exogenous injection of interleukin-1 in some tumor models (47). In contrast, NLRP3 inflammasome production of interleukin 1 is correlated with an increased tumor burden and tumor progression in colorectal cancer.(55) This finding is supported by other data illustrating that IL-1β signaling in epithelial cells drives stemness and tumor progression.(56) For instance, in prostate cancer models, transient upregulation of interleukin-1 promotes prostatic proliferative inflammatory atrophy and leads to aggressive prostate adenocarcinoma.(57) The commonality in all of the above studies is that IL-1β appears to interact predominantly with the myeloid compartment, with less pronounced effects on T cells, consistent with the findings described here.(58)

In early tumor treatment models, the addition of anti-IL-1β to anti-PD-1 resulted in additive effects on tumor outgrowth and improved T cell mediated tumor killing.(15) One strength of our work is that we studied later, well-established tumors, and found that myeloid compartment remodeling is achievable. This suggests that even earlier treatment might be preferable; in that regard an ongoing clinical study is evaluating combination therapy with spartalizumab (anti-PD-1) plus canakinumab (anti-IL-1β) prior to nephrectomy for patients with high-risk RCC with the goal of decreasing intratumoral MDSCs and decreasing the risk of relapse (NCT04028245). Consistent with this hypothesis, a query of interleukin-1β gene expression through TCGA illustrates that high IL-1β RNA expression is associated with worse overall survival (Supplemental Figure 10). One potentially unique implication of our data is that IL-1β might be upstream of interleukin-8 homologs; this is important because elevated IL-8 levels are associated with lack of response to anti-PD-1.(59) Clinical studies blocking IL-8 in combination with anti-PD-1 are ongoing (NCT03400332, NCT03689699, NCT04123379).(60,61)

A potential limitation of our study is that RENCA as tumor model lacks the mutations commonly associated with ccRCC including VHL loss, PBRM-1, BAP-1, and SETD2. Despite the shortcomings of RENCA as a genetic model of RCC, this tumor contains a robust myeloid cell infiltrate which may reflect more aggressive human RCC phenotypes. For instance, transcriptomic profiling of human RCC from the COMPARZ trial clearly showed worse overall survival for patients with angiogenesis^{lo}, macrophage^{hi} gene signatures which was largely independent of mutational status in VHL, PBRM1, and BAP1.(62) Hence, the dense myeloid infiltrate observed in RENCA may be similarly reflective of immunosuppressive tumor microenvironments associated with treatment refractory RCCs. To assess the relative contribution of combination cabozantinib and anti-IL-1β on tumor growth in a tumor type with less TAM infiltrate, we also evaluated this combination in the MC38 CRC model (Supplemental Figure 9). We did not note statistically significant changes in tumor outgrowth with cabozantinib, anti-IL-1β, or combination treatment in this model. These data suggest that combination anti-IL-1β with a VEGF targeted TKI is not likely to be a universal immune combination therapy in human RCC, and may require a level of patient selection. Therapeutics that rely on myeloid remodeling may be central to future RCC treatment selection, particularly as novel biomarkers are tested that reflect the relative degree of macrophage infiltration.

Finally, as IL-1β is also known to promote angiogenesis(63,64), it was interesting to find that treating established tumors with IL-1β plus cabozantinib led to a marked reduction in tumor growth and increased M1-TAM infiltration. In summary, our data inform future clinical trial development, by supporting the notion that anti-IL-1β might have activity in RCC, either in combination with anti-PD-1 or in combination with the TKI cabozantinib.

Supplementary Material

Refer to Web version on PubMed Central for supplementary material.

Acknowledgements:

The authors would like to acknowledge Dr. Siu-Hong Ho and Dr. Lu Caisheng of the Flow Cytometry Core Facility at the Herbert Irving Comprehensive Cancer Center.

Financial Support: These studies were supported by the ASCO Conquer Cancer Foundation Young Investigator Award, National Institutes of Health (NIH) grants R01 CA127153, 1P50CA58236-15 and P30CA006973, and CUMC institutional funds to CGD.

References:

1. Siegel RL, Miller KD, Jemal A. Cancer statistics, 2020. CA Cancer J Clin 2020;70(1):7–30 doi 10.3322/caac.21590. [PubMed: 31912902]
2. Klapper JA, Downey SG, Smith FO, Yang JC, Hughes MS, Kammula US, et al. High-dose interleukin-2 for the treatment of metastatic renal cell carcinoma : a retrospective analysis of response and survival in patients treated in the surgery branch at the National Cancer Institute between 1986 and 2006. Cancer 2008;113(2):293–301 doi 10.1002/cncr.23552. [PubMed: 18457330]
3. Aggen DH, Drake CG, Rini BI. Targeting PD-1 or PD-L1 in Metastatic Kidney Cancer - Combination Therapy in the First Line Setting. Clin Cancer Res 2020 doi 10.1158/1078-0432.CCR-19-3323.
4. Motzer RJ, Tannir NM, McDermott DF, Aren Frontera O, Melichar B, Choueiri TK, et al. Nivolumab plus Ipilimumab versus Sunitinib in Advanced Renal-Cell Carcinoma. N Engl J Med 2018;378(14):1277–90 doi 10.1056/NEJMoa1712126. [PubMed: 29562145]
5. Motzer RJ, Penkov K, Haanen J, Rini B, Albiges L, Campbell MT, et al. Avelumab plus Axitinib versus Sunitinib for Advanced Renal-Cell Carcinoma. N Engl J Med 2019;380(12):1103–15 doi 10.1056/NEJMoa1816047. [PubMed: 30779531]
6. Rini BI, Plimack ER, Stus V, Gafanov R, Hawkins R, Nosov D, et al. Pembrolizumab plus Axitinib versus Sunitinib for Advanced Renal-Cell Carcinoma. N Engl J Med 2019;380(12):1116–27 doi 10.1056/NEJMoa1816714. [PubMed: 30779529]
7. Bruchard M, Mignot G, Derangere V, Chalmin F, Chevriaux A, Vegran F, et al. Chemotherapy-triggered cathepsin B release in myeloid-derived suppressor cells activates the Nlrp3 inflammasome and promotes tumor growth. Nat Med 2013;19(1):57–64 doi 10.1038/nm.2999. [PubMed: 23202296]
8. Drake CG, Stein MN. The Immunobiology of Kidney Cancer. J Clin Oncol 2018:JCO2018792648 doi 10.1200/JCO.2018.79.2648.
9. Najjar YG, Rayman P, Jia X, Pavicic PG Jr., Rini BI, Tannenbaum C, et al. Myeloid-Derived Suppressor Cell Subset Accumulation in Renal Cell Carcinoma Parenchyma Is Associated with Intratumoral Expression of IL1beta, IL8, CXCL5, and Mip-1alpha. Clin Cancer Res 2017;23(9):2346–55 doi 10.1158/1078-0432.CCR-15-1823. [PubMed: 27799249]
10. Rider P, Carmi Y, Guttman O, Braiman A, Cohen I, Voronov E, et al. IL-1alpha and IL-1beta recruit different myeloid cells and promote different stages of sterile inflammation. J Immunol 2011;187(9):4835–43 doi 10.4049/jimmunol.1102048. [PubMed: 21930960]
11. Dinarello CA. Why not treat human cancer with interleukin-1 blockade? Cancer and Metastasis Reviews 2010;29(2):317–29 doi 10.1007/s10555-010-9229-0. [PubMed: 20422276]
12. Voronov E, Shouval DS, Krelin Y, Cagnano E, Benharroch D, Iwakura Y, et al. IL-1 is required for tumor invasiveness and angiogenesis. Proc Natl Acad Sci U S A 2003;100(5):2645–50 doi 10.1073/pnas.0437939100. [PubMed: 12598651]
13. Dinarello CA, Simon A, van der Meer JWM. Treating inflammation by blocking interleukin-1 in a broad spectrum of diseases. Nature Reviews Drug Discovery 2012;11(8):633–52 doi 10.1038/nrd3800. [PubMed: 22850787]
14. Krelin Y, Voronov E, Dotan S, Elkabets M, Reich E, Fogel M, et al. Interleukin-1beta-driven inflammation promotes the development and invasiveness of chemical carcinogen-induced tumors. Cancer Res 2007;67(3):1062–71 doi 10.1158/0008-5472.CAN-06-2956. [PubMed: 17283139]

15. Kaplanov I, Carmi Y, Kornetsky R, Shemesh A, Shurin GV, Shurin MR, et al. Blocking IL-1beta reverses the immunosuppression in mouse breast cancer and synergizes with anti-PD-1 for tumor abrogation. Proc Natl Acad Sci U S A 2019;116(4):1361–9 doi 10.1073/pnas.1812266115. [PubMed: 30545915]
16. Wu TC, Xu K, Martinek J, Young RR, Banchereau R, George J, et al. IL1 Receptor Antagonist Controls Transcriptional Signature of Inflammation in Patients with Metastatic Breast Cancer. Cancer Res 2018;78(18):5243–58 doi 10.1158/0008-5472.CAN-18-0413. [PubMed: 30012670]
17. Tannenbaum CS, Rayman PA, Pavicic PG, Kim JS, Wei W, Polefko A, et al. Mediators of Inflammation-Driven Expansion, Trafficking, and Function of Tumor-Infiltrating MDSCs. Cancer Immunology Research 2019:canimm.0578.2018 doi 10.1158/2326-6066.CIR-18-0578.
18. Chittezhath M, Dhillon MK, Lim JY, Laoui D, Shalova IN, Teo YL, et al. Molecular profiling reveals a tumor-promoting phenotype of monocytes and macrophages in human cancer progression. Immunity 2014;41(5):815–29 doi 10.1016/j.immuni.2014.09.014. [PubMed: 25453823]
19. Ridker PM, Everett BM, Thuren T, MacFadyen JG, Chang WH, Ballantyne C, et al. Antiinflammatory Therapy with Canakinumab for Atherosclerotic Disease. N Engl J Med 2017;377(12):1119–31 doi 10.1056/NEJMoa1707914. [PubMed: 28845751]
20. Ridker PM, MacFadyen JG, Thuren T, Everett BM, Libby P, Glynn RJ, et al. Effect of interleukin-1beta inhibition with canakinumab on incident lung cancer in patients with atherosclerosis: exploratory results from a randomised, double-blind, placebo-controlled trial. Lancet 2017;390(10105):1833–42 doi 10.1016/S0140-6736(17)32247-X. [PubMed: 28855077]
21. Muroyama Y, Nirschl TR, Kochel CM, Lopez-Bujanda Z, Theodros D, Mao W, et al. Stereotactic Radiotherapy Increases Functionally Suppressive Regulatory T Cells in the Tumor Microenvironment. Cancer Immunol Res 2017;5(11):992–1004 doi 10.1158/2326-6066.CIR-17-0040. [PubMed: 28970196]
22. Marciscano AE, Ghasemzadeh A, Nirschl TR, Theodros D, Kochel CM, Francica BJ, et al. Elective Nodal Irradiation Attenuates the Combinatorial Efficacy of Stereotactic Radiation Therapy and Immunotherapy. Clinical Cancer Research 2018;24(20):5058 doi 10.1158/1078-0432.CCR-17-3427. [PubMed: 29898992]
23. Keane TM, Goodstadt L, Danecek P, White MA, Wong K, Yalcin B, et al. Mouse genomic variation and its effect on phenotypes and gene regulation. Nature. Volume 4772011. p 289–94.
24. McDavid A, Finak G, Chattopadyay PK, Dominguez M, Lamoreaux L, Ma SS, et al. Data exploration, quality control and testing in single-cell qPCR-based gene expression experiments. Bioinformatics 2013;29(4):461–7 doi 10.1093/bioinformatics/bts714. [PubMed: 23267174]
25. Ayers M, Lunceford J, Nebozhyn M, Murphy E, Loboda A, Kaufman DR, et al. IFN-γ–related mRNA profile predicts clinical response to PD-1 blockade. The Journal of Clinical Investigation 2017;127(8):2930–40 doi 10.1172/JCI91190. [PubMed: 28650338]
26. Shaughnessy MJ, Murray KS, La Rosa SP, Budhu S, Merghoub T, Somma A, et al. Systemic Antitumor Immunity by PD-1/PD-L1 Inhibition Is Potentiated by Vascular-Targeted Photodynamic Therapy of Primary Tumors. Clinical Cancer Research 2018;24(3):592 doi 10.1158/1078-0432.CCR-17-0186. [PubMed: 28954788]
27. Yu JW, Bhattacharya S, Yanamandra N, Kilian D, Shi H, Yadavilli S, et al. Tumor-immune profiling of murine syngeneic tumor models as a framework to guide mechanistic studies and predict therapy response in distinct tumor microenvironments. PLoS One 2018;13(11):e0206223–e doi 10.1371/journal.pone.0206223. [PubMed: 30388137]
28. Bronte V, Brandau S, Chen S-H, Colombo MP, Frey AB, Greten TF, et al. Recommendations for myeloid-derived suppressor cell nomenclature and characterization standards. Nature Communications 2016;7:12150 doi 10.1038/ncomms12150.
29. Cassetta L, Baekkevold ES, Brandau S, Bujko A, Cassatella MA, Dorhoi A, et al. Deciphering myeloid-derived suppressor cells: isolation and markers in humans, mice and non-human primates. Cancer Immunol Immunother 2019;68(4):687–97 doi 10.1007/s00262-019-02302-2. [PubMed: 30684003]
30. Hol J, Wilhelmsen L, Haraldsen G. The murine IL-8 homologues KC, MIP-2, and LIX are found in endothelial cytoplasmic granules but not in Weibel-Palade bodies. Journal of Leukocyte Biology 2010;87(3):501–8 doi 10.1189/jlb.0809532. [PubMed: 20007247]

31. Fu W, Zhang Y, Zhang J, Chen W-F. Cloning and characterization of mouse homolog of the CXC chemokine receptor CXCR1. Cytokine 2005;31(1):9–17 doi 10.1016/j.cyto.2005.02.005. [PubMed: 15967374]
32. Rovai LE, Herschman HR, Smith JB. The murine neutrophil-chemoattractant chemokines LIX, KC, and MIP-2 have distinct induction kinetics, tissue distributions, and tissue-specific sensitivities to glucocorticoid regulation in endotoxemia. Journal of Leukocyte Biology 1998;64(4):494–502 doi 10.1002/jlb.64.4.494. [PubMed: 9766630]
33. Bozic CR, Gerard NP, von Uexkull-Guldenband C, Kolakowski LF, Conklyn MJ, Breslow R, et al. The murine interleukin 8 type B receptor homologue and its ligands. Expression and biological characterization. Journal of Biological Chemistry 1994;269(47):29355–8.
34. Lopez-Bujanda ZA, Haffner MC, Chaimowitz MG, Chowdhury N, Venturini NJ, Obradovic A, et al. Castration-mediated IL-8 Promotes Myeloid Infiltration and Prostate Cancer Progression. bioRxiv 2019:651083 doi 10.1101/651083.
35. Ashburner M, Ball CA, Blake JA, Botstein D, Butler H, Cherry JM, et al. Gene ontology: tool for the unification of biology. The Gene Ontology Consortium. Nat Genet 2000;25(1):25–9 doi 10.1038/75556. [PubMed: 10802651]
36. The Gene Ontology Consortium. The Gene Ontology Resource: 20 years and still GOing strong. Nucleic Acids Research 2018;47(D1):D330–D8 doi 10.1093/nar/gky1055.
37. Escudier B Combination Therapy as First-Line Treatment in Metastatic Renal-Cell Carcinoma. New England Journal of Medicine 2019;380(12):1176–8 doi 10.1056/NEJMe1900887.
38. Yakes FM, Chen J, Tan J, Yamaguchi K, Shi Y, Yu P, et al. Cabozantinib (XL184), a novel MET and VEGFR2 inhibitor, simultaneously suppresses metastasis, angiogenesis, and tumor growth. Mol Cancer Ther 2011;10(12):2298–308 doi 10.1158/1535-7163.MCT-11-0264. [PubMed: 21926191]
39. Balkwill F, Mantovani A. Inflammation and cancer: back to Virchow? Lancet 2001;357(9255):539–45 doi 10.1016/S0140-6736(00)04046-0. [PubMed: 11229684]
40. LaFleur MW, Muroyama Y, Drake CG, Sharpe AH. Inhibitors of the PD-1 Pathway in Tumor Therapy. The Journal of Immunology 2018;200(2):375 doi 10.4049/jimmunol.1701044. [PubMed: 29311378]
41. Cahill CM, Rogers JT. Interleukin (IL) 1β Induction of IL-6 Is Mediated by a Novel Phosphatidylinositol 3-Kinase-dependent AKT/IκB Kinase α Pathway Targeting Activator Protein-1. Journal of Biological Chemistry 2008;283(38):25900–12 doi 10.1074/jbc.M707692200.
42. Mantovani A, Dinarello CA, Molgora M, Garlanda C. Interleukin-1 and Related Cytokines in the Regulation of Inflammation and Immunity. Immunity 2019;50(4):778–95 doi 10.1016/j.immuni.2019.03.012. [PubMed: 30995499]
43. Tsukamoto H, Fujieda K, Miyashita A, Fukushima S, Ikeda T, Kubo Y, et al. Combined Blockade of IL6 and PD-1/PD-L1 Signaling Abrogates Mutual Regulation of Their Immunosuppressive Effects in the Tumor Microenvironment. Cancer Res 2018;78(17):5011–22 doi 10.1158/0008-5472.CAN-18-0118. [PubMed: 29967259]
44. Weber JS, Sznol M, Sullivan RJ, Blackmon S, Boland G, Kluger HM, et al. A Serum Protein Signature Associated with Outcome after Anti-PD-1 Therapy in Metastatic Melanoma. Cancer Immunol Res 2018;6(1):79–86 doi 10.1158/2326-6066.CIR-17-0412. [PubMed: 29208646]
45. Bilusic M, Heery CR, Collins JM, Donahue RN, Palena C, Madan RA, et al. Phase I trial of HuMax-IL8 (BMS-986253), an anti-IL-8 monoclonal antibody, in patients with metastatic or unresectable solid tumors. J Immunother Cancer 2019;7(1):240 doi 10.1186/s40425-019-0706-x. [PubMed: 31488216]
46. Perez-Ruiz E, Minute L, Otano I, Alvarez M, Ochoa MC, Belsue V, et al. Prophylactic TNF blockade uncouples efficacy and toxicity in dual CTLA-4 and PD-1 immunotherapy. Nature 2019;569(7756):428–32 doi 10.1038/s41586-019-1162-y. [PubMed: 31043740]
47. Czystowska M, Gooding W, Szczepanski MJ, Lopez-Abaitero A, Ferris RL, Johnson JT, et al. The Immune Signature of $CD8^{+}CCR7^{+}$ T Cells in the Peripheral Circulation Associates with Disease Recurrence in Patients with HNSCC. Clinical Cancer Research 2013;19(4):889 doi 10.1158/1078-0432.CCR-12-2191. [PubMed: 23363813]

48. Takeuchi Y, Tanemura A, Tada Y, Katayama I, Kumanogoh A, Nishikawa H. Clinical response to PD-1 blockade correlates with a sub-fraction of peripheral central memory CD4+ T cells in patients with malignant melanoma. Int Immunol 2018;30(1):13–22 doi 10.1093/intimm/dxx073. [PubMed: 29294043]
49. Gubin MM, Esaulova E, Ward JP, Malkova ON, Runci D, Wong P, et al. High-Dimensional Analysis Delineates Myeloid and Lymphoid Compartment Remodeling during Successful Immune-Checkpoint Cancer Therapy. Cell 2018;175(4):1014–30 e19 doi 10.1016/j.cell.2018.09.030. [PubMed: 30343900]
50. Chevrier S, Levine JH, Zanotelli VRT, Silina K, Schulz D, Bacac M, et al. An Immune Atlas of Clear Cell Renal Cell Carcinoma. Cell 2017;169(4):736–49 e18 doi 10.1016/j.cell.2017.04.016. [PubMed: 28475899]
51. Bunt SK, Sinha P, Clements VK, Leips J, Ostrand-Rosenberg S. Inflammation Induces Myeloid-Derived Suppressor Cells that Facilitate Tumor Progression. The Journal of Immunology 2006;176(1):284 doi 10.4049/jimmunol.176.1.284. [PubMed: 16365420]
52. North RJ, Neubauer RH, Huang JJ, Newton RC, Loveless SE. Interleukin 1-induced, T cell-mediated regression of immunogenic murine tumors. Requirement for an adequate level of already acquired host concomitant immunity. J Exp Med 1988;168(6):2031–43 doi 10.1084/jem.168.6.2031. [PubMed: 3143799]
53. Haabeth OA, Lorvik KB, Hammarstrom C, Donaldson IM, Haraldsen G, Bogen B, et al. Inflammation driven by tumour-specific Th1 cells protects against B-cell cancer. Nat Commun 2011;2:240 doi 10.1038/ncomms1239. [PubMed: 21407206]
54. Haabeth OA, Lorvik KB, Yagita H, Bogen B, Corthay A. Interleukin-1 is required for cancer eradication mediated by tumor-specific Th1 cells. Oncoimmunology 2016;5(1):e1039763 doi 10.1080/2162402X.2015.1039763. [PubMed: 26942052]
55. Dmitrieva-Posocco O, Dzutsev A, Posocco DF, Hou V, Yuan W, Thovarai V, et al. Cell-Type-Specific Responses to Interleukin-1 Control Microbial Invasion and Tumor-Elicited Inflammation in Colorectal Cancer. Immunity 2019;50(1):166–80 e7 doi 10.1016/j.immuni.2018.11.015. [PubMed: 30650375]
56. Li Y, Wang L, Pappan L, Galliher-Beckley A, Shi J. IL-1beta promotes stemness and invasiveness of colon cancer cells through Zeb1 activation. Mol Cancer 2012;11:87 doi 10.1186/1476-4598-11-87. [PubMed: 23174018]
57. Ashok A, Keener R, Rubenstein M, Stookey S, Bajpai S, Hicks J, et al. Consequences of interleukin 1beta-triggered chronic inflammation in the mouse prostate gland: Altered architecture associated with prolonged CD4(+) infiltration mimics human proliferative inflammatory atrophy. Prostate 2019;79(7):732–45 doi 10.1002/pros.23784. [PubMed: 30900284]
58. Mantovani A, Barajon I, Garlanda C. IL-1 and IL-1 regulatory pathways in cancer progression and therapy. Immunol Rev 2018;281(1):57–61 doi 10.1111/imr.12614. [PubMed: 29247996]
59. Sanmamed MF, Perez-Gracia JL, Schalper KA, Fusco JP, Gonzalez A, Rodriguez-Ruiz ME, et al. Changes in serum interleukin-8 (IL-8) levels reflect and predict response to anti-PD-1 treatment in melanoma and non-small-cell lung cancer patients. Annals of Oncology 2017;28(8):1988–95 doi 10.1093/annonc/mdx190. [PubMed: 28595336]
60. Bilusic M, Heery CR, Collins JM, Donahue RN, Palena C, Madan RA, et al. Phase I trial of HuMax-IL8 (BMS-986253), an anti-IL-8 monoclonal antibody, in patients with metastatic or unresectable solid tumors. Journal for ImmunoTherapy of Cancer 2019;7(1):240 doi 10.1186/s40425-019-0706-x. [PubMed: 31488216]
61. Dallos M, Aggen DH, Hawley J, Lim EA, Stein MN, Kelly WK, et al. A randomized phase Ib/II study of nivolumab with or without BMS-986253 in combination with a short course of ADT in men with castration-sensitive prostate cancer (MAGIC-8). Journal of Clinical Oncology 2019;37(7_suppl):TPS329–TPS doi 10.1200/JCO.2019.37.7_suppl.TPS329.
62. Hakimi AA, Voss MH, Kuo F, Sanchez A, Liu M, Nixon BG, et al. Transcriptomic Profiling of the Tumor Microenvironment Reveals Distinct Subgroups of Clear Cell Renal Cell Cancer: Data from a Randomized Phase III Trial. Cancer Discovery 2019;9(4):510 doi 10.1158/2159-8290.CD-18-0957. [PubMed: 30622105]

63. Voronov E, Shouval DS, Krelin Y, Cagnano E, Benharroch D, Iwakura Y, et al. IL-1 is required for tumor invasiveness and angiogenesis. Proceedings of the National Academy of Sciences 2003;100(5):2645 doi 10.1073/pnas.0437939100.

64. Song X, Voronov E, Dvorkin T, Fima E, Cagnano E, Benharroch D, et al. Differential Effects of IL-1α and IL-1β on Tumorigenicity Patterns and Invasiveness. The Journal of Immunology 2003;171(12):6448 doi 10.4049/jimmunol.171.12.6448. [PubMed: 14662844]

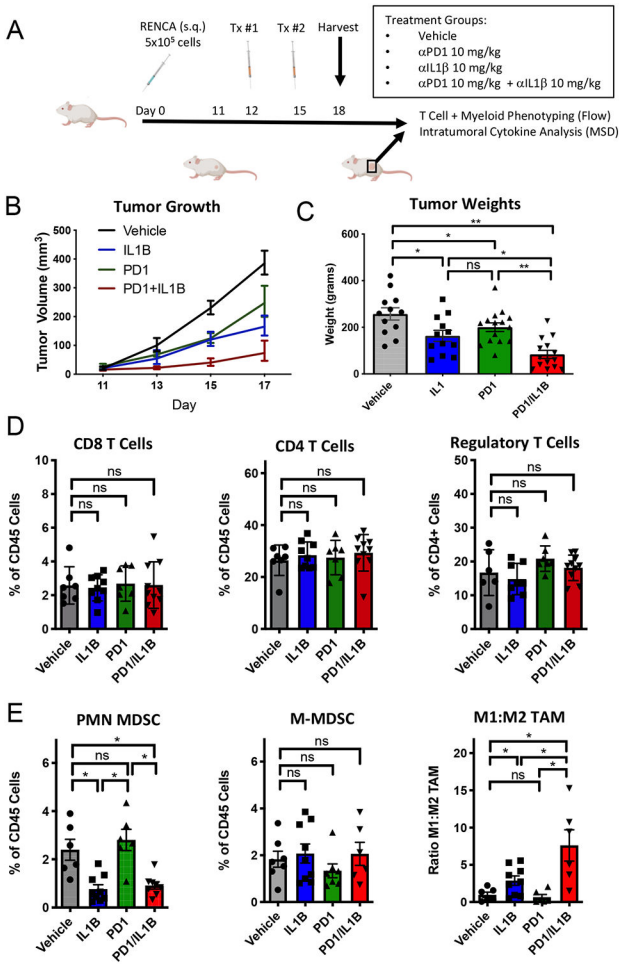

Figure 1. Combination anti-IL1β and anti-PD-1 treatment delays RENCA tumor growth.

A) Treatment schema for murine experiments. B) Tumor growth beginning on day +12 as measured by calipers (n=10/group). IL1B (anti-IL-1β antibody), PD1 (anti-PD-1 antibody), PD1 + IL1B (combination anti-PD-1 and anti-IL-1β). C) Day +18 tumor weights (n = 10/group). D) T cell immunophenotyping from RENCA treated tumors on Day +18. E) Myeloid cell populations quantified by flow cytometry (n = 6/group). PMN-MDSC defined as CD45+, CD11b+, Ly6Cint, Ly6GHi cells. M-MDSC defined as CD45+, CD11b+, Ly6CHi, MHCII+. Macrophages defined as CD45+, CD11b+, F4/80+ with M1 (MHC II (I-Ek) Hi) and M2 (MHC II low)). E) Data are representative of 3 separate experiments. Mice from vehicle and IL-1b were used as controls for flow cytometry experiments done in parallel in figure 3. Error bars are mean +/− standard error of mean. * $P < 0.05$, ** $P < 0.001$

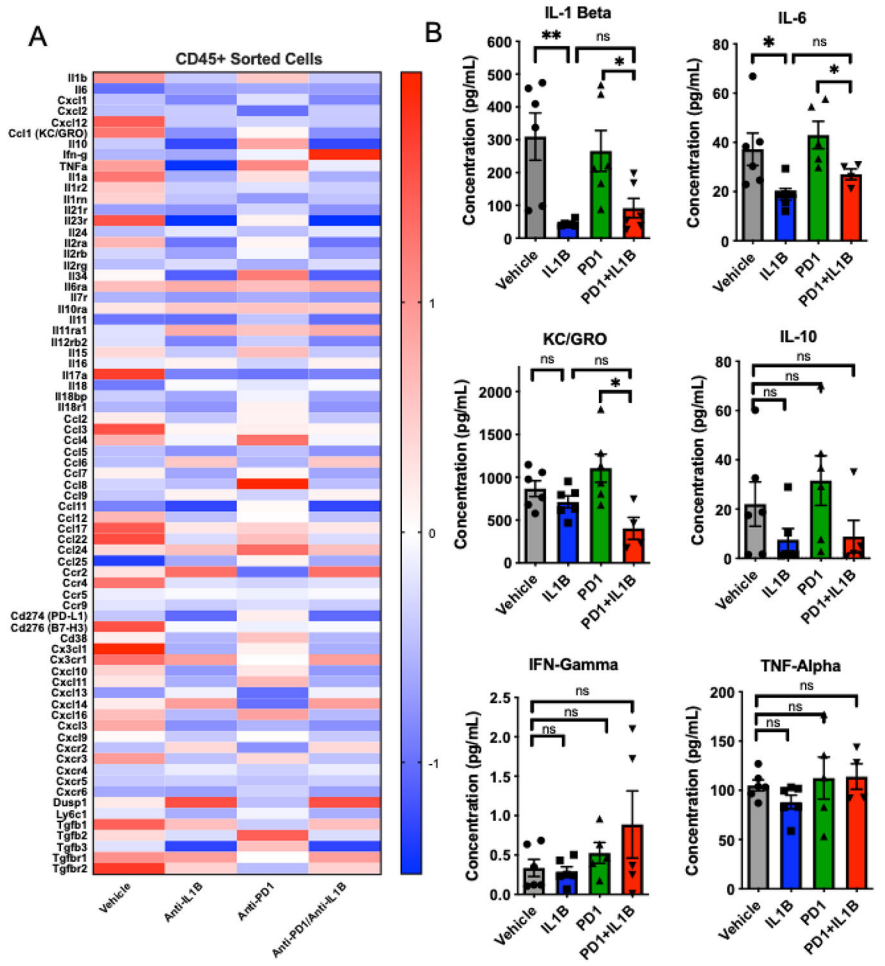

Figure 2. Anti-Interleukin-1 β in combination with anti-PD1 modulates intratumoral cytokines.

A) Z-scores of differentially expressed genes from CD45+ intratumoral immune cells (n=3 mice/group). B) Mesoscale quantification of intratumoral cell lysates of select cytokines using U-Plex panel. (n=5 mice/group). The RNAseq data shown for vehicle and IL-1beta is identical to that in figure 4, and this data set was used as a control for other comparators. Error bars are mean +/− standard error of mean. *P< 0.05, ** P < 0.005

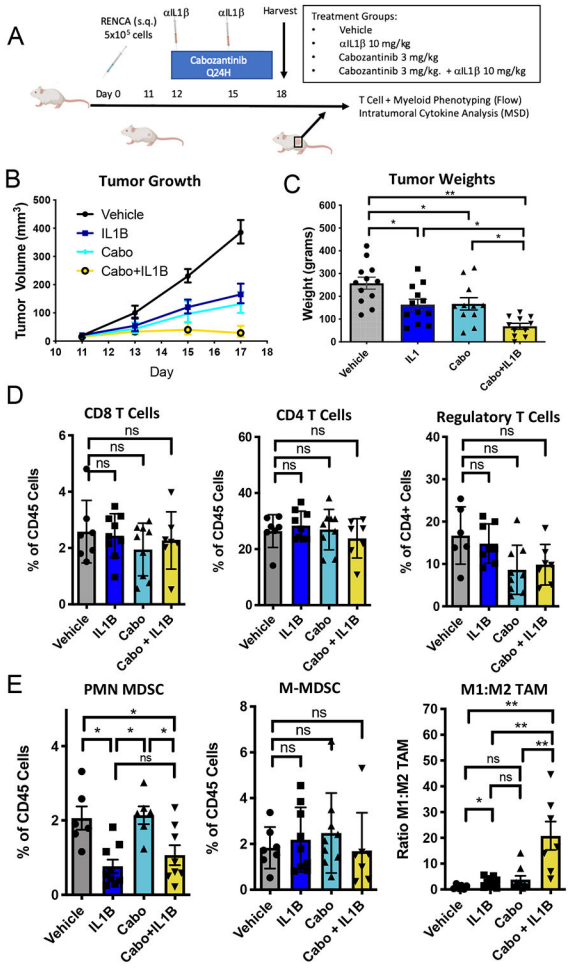

Figure 3. Anti-Interleukin-1β augments the response to cabozantinib.

Mice were treated with cabozantinib daily beginning on Day +12 in combination with every 3 day anti-IL-1β. A) Tumor growth curves after treatment with vehicle, anti-IL1β (IL1B), cabozantinib (3 mg/kg) or cabozantinib + anti-IL-1β (Cabo+IL1B). B) Tumors on day +8 after initiating treatment. C) Tumor weights on day +8 after treatment (n=10/group). Representative of 3 separate experiments. D) T cell immunophenotyping from RENCA treated tumors on Day +18. E) Myeloid cell populations quantified by flow cytometry (n = 6/group). Data are representative of 3 separate experiments. Vehicle and anti-IL-1β treated mice shown are identical to the mice used in figure 1 to minimize the number of mice used. Mice from vehicle and IL-1beta were used as controls for flow cytometry experiments that were performed in parallel with the experiments in figure 1. Error bars are mean +/− standard error of mean. * $P < 0.05$, ** $P < 0.005$

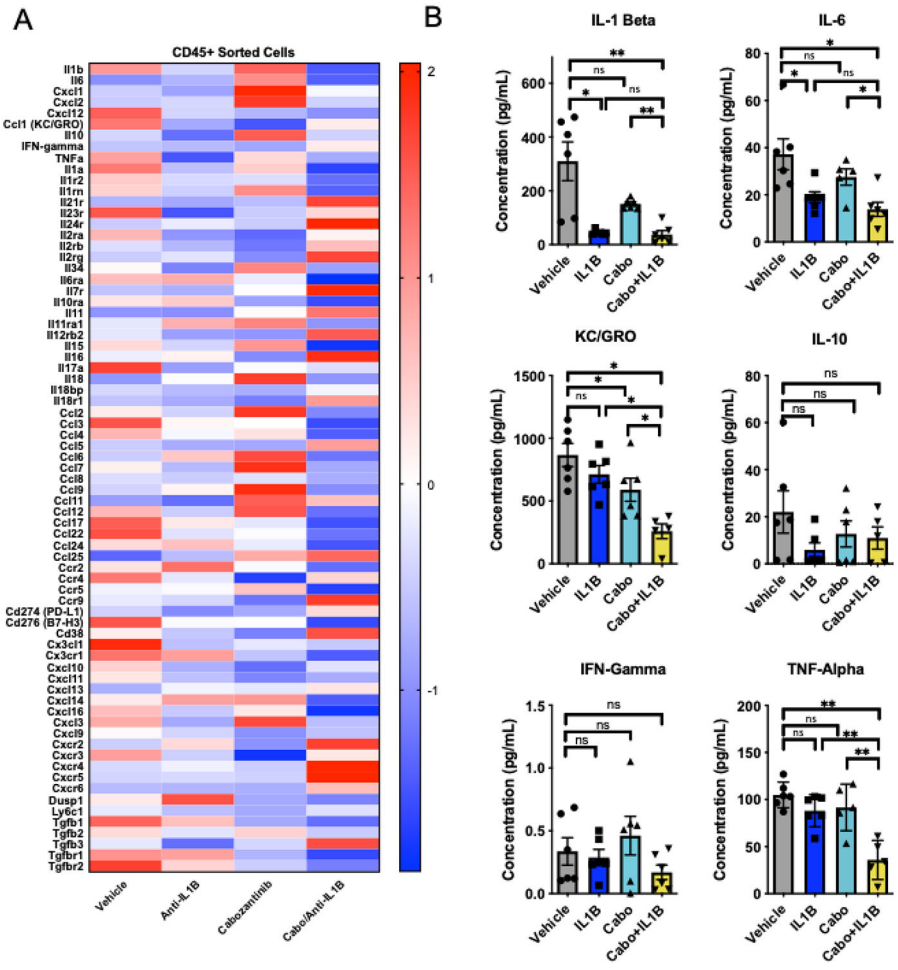

Figure 4. Combination cabozantinib and anti-Interleukin-1β modulate intratumoral cytokines.

A) Z-scores of differentially expressed genes from CD45+ intratumoral immune cells (n=3 mice/group). B) Mesoscale quantification of intratumoral cell lysates of select cytokines using U-Plex panel. (n=5 mice/group). Error bars are mean +/− standard error of mean. Data for vehicle and anti-IL-1β are from the same sorted immune cells described in figure 2. *P< 0.05, ** P < 0.005

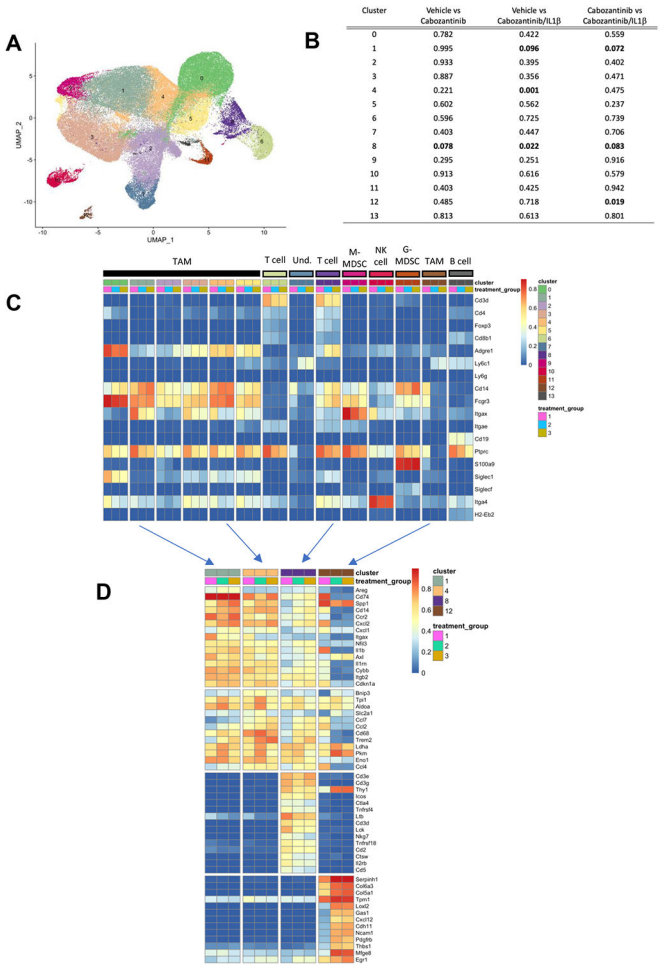

Cluster	Vehicle vs Cabozantinib	Vehicle vs Cabozantinib/IL1β	Cabozantinib vs Cabozantinib/IL1β
0	0.782	0.422	0.559
1	0.995	**0.096**	**0.072**
2	0.933	0.395	0.402
3	0.887	0.356	0.471
4	0.221	**0.001**	0.475
5	0.602	0.562	0.237
6	0.596	0.725	0.739
7	0.403	0.447	0.706
8	**0.078**	**0.022**	**0.083**
9	0.295	0.251	0.916
10	0.913	0.616	0.579
11	0.403	0.425	0.942
12	0.485	0.718	**0.019**
13	0.813	0.613	0.801

Figure 5. Myeloid changes within the tumor microenvironment identified by high-dimensional single-cell analysis following cabozantinib or cabozantinib and anti-IL1β treatment.

A). Clustering of sorted CD45+ intratumoral immune cells visualized by UMAP from 9 tumors (3 vehicle, 3 cabozantinib, and 3 cabozantinib/IL1B treated tumors) reveals distinct immune cell populations. B) Gene expression profiles of select genes identify distinct immune cell clusters. C) Gene expression profiles across treatment groups. Clusters 6 and 8 express T cell specific genes. Treatment group 1 = vehicle, Treatment group 2 = cabozantinib, Treatment group 3 = Cabozantinib + IL1B. Clusters 0–5, 7, 9–12 correspond to myeloid cells within the TME. D) Top 10 to 15 differentially expressed genes in clusters 1, 8, and 12 from single-cell RNAseq. (n=3 tumors/group from each treatment group).

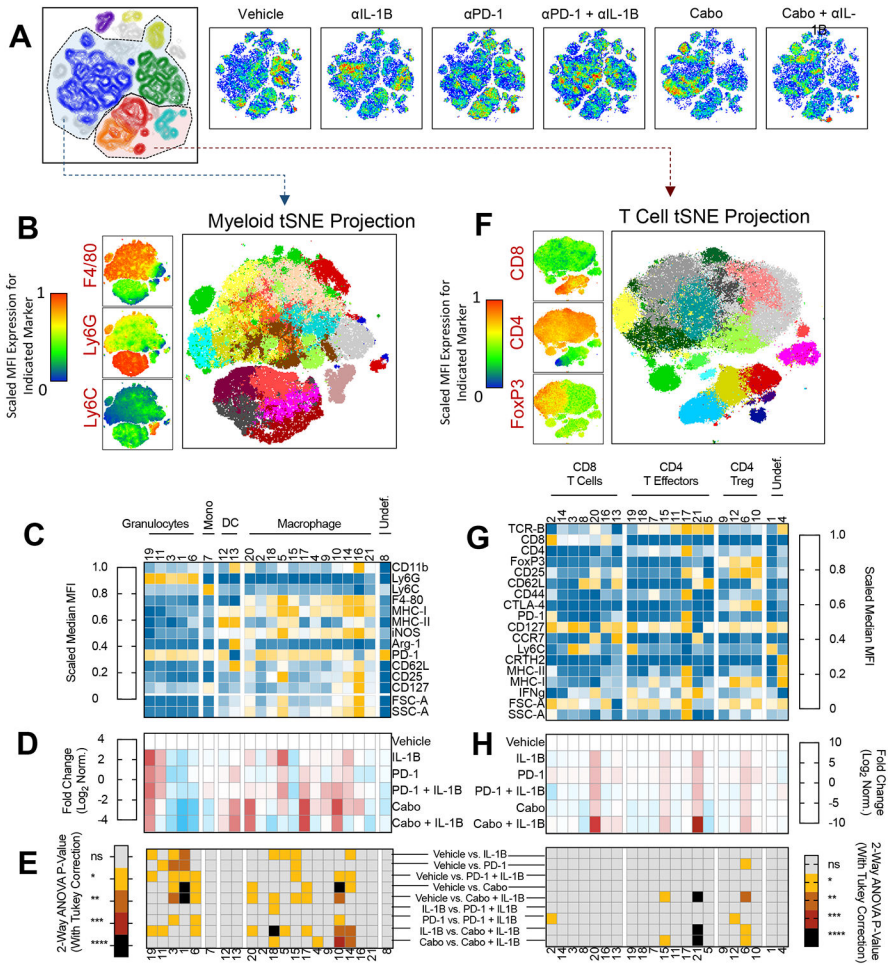

Figure 6. Myeloid changes within the tumor microenvironment following combination anti-interleukin-1 beta immunotherapy.

A). TSNE clustering of CD45+ immune cells from spectral cytometry (n= 8–10 mice/group). Cell Density plots shows for each treatment group (blue is low density, red is highest density) B) Phenograph clustering of intratumoral myeloid cell populations for all mice across treatment groups. Representative marker expression for F4/80, Ly6G, and F4/80 at left and myeloid TSNE projection showing 21 clusters (right). C) Relative MFI for each myeloid marker across phenograph clusters. D) Fold–change of myeloid cluster frequency by treatment group. E) 2-way ANOVA of select treatment groups with Tukey correction to show statistically significant changes in cluster frequency. Treatment group comparisons are as indicated at right. F) Phenograph clustering of intratumoral lymphoid populations for all mice across treatment groups. Representative marker expression for CD4, CD8, and FoxP3 at left and T cell specific TSNE projection showing 21 clusters (right). G) Relative frequency for each marker across phonograph clusters. H) Fold-change of lymphoid cluster frequency by treatment group. E) (at right) 2-way ANOVA of select treatment groups with Tukey correction to show statistically significant changes in cluster frequency. * $P < 0.05$, ** $P < 0.01$, *** $P < 0.001$, **** $P < 0.0001$